Electronic Supplementary Material (ESI) for Physical Chemistry Chemical Physics.

Supporting Information

How fast is optically induced electron transfer in organic mixed valence systems?

Christoph Lambert,* Michael Moos, Alexander Schmiedel, Marco Holzapfel, Julian Schäfer, Martin Kess, Volker Engel

Experimental

Compounds **1** and **2** have been synthesized according to literature[1] and compound **3** according to ref [2].

Cyclic voltammetry

In order to determine the comproportionation constant cyclic voltammetry of compound **1** was performed in DCM and MeCN with an electrolyte concentration of 0.1 mol•l^{-1}. [*n*-Bu_4N][PF_6] was synthesized according to literature[3], DCM and MeCN were distilled from CaH_2 prior to use.

A flame dried and argon flushed three electrode setup (1 mm Pt-disc working electrode, Pt-wire counter electrode, leak free Ag/AgCl reference electrode from Warner Instruments) was used in combination with a Reference 600 potentiostat (Gamry) and a Faraday cage.

All voltammograms were referenced vs. Fc/Fc^+ for better comparison.

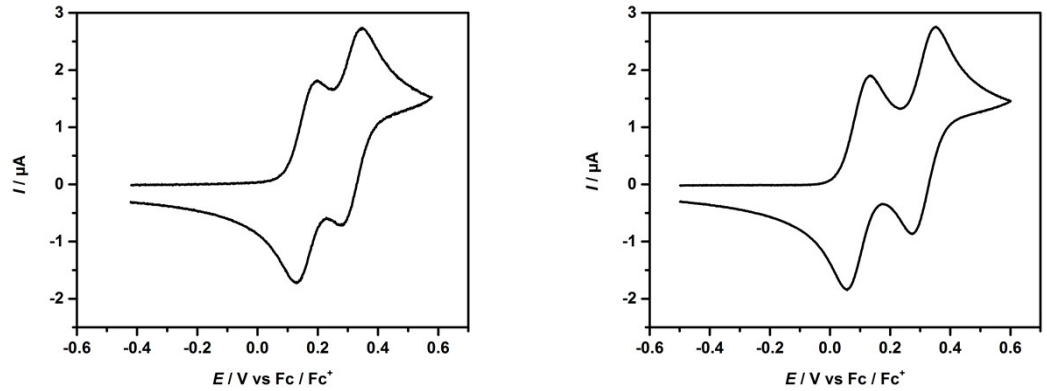

Figure S1: Cyclic voltammograms of **1** in 0.1 M [*n*-Bu_4N][PF_6]/MeCN (left side) and 0.1 M [*n*-Bu_4N][PF_6]/DCM (right side) at 250 mV s^{-1} vs. Fc/Fc^+.

Table S1: Half wave potentials of the first and second oxidation of the triarylamine-moieties ($E^{Ox}_{1/2}$).

compound	solvent	$E^{Ox}_{1/2}$ / V (TAA_1)	$E^{Ox}_{1/2}$ / V (TAA_2)	$\Delta E_{1/2}$ / V
1	MeCN	0.166	0.316	0.150
1	DCM	0.102	0.316	0.214

Redox Titrations

Redox titrations monitored by UV/Vis/NIR spectroscopy were performed in four different solvents using a Cary 5000 absorption spectrometer (Agilent technologies) and 10×10 mm quartz-cuvettes with Teflon stopper (Starna). Spectrophotometric solvents (DCM, MeCN) were used as purchased (Merck Uvasol). PhCN and $PhNO_2$ were distilled and stored over molecular sieves (3 Å) prior to use. $SbCl_5$ (Acros Organics) was used as oxidant in all cases. Because of instability $SbCl_5$ was dissolved in DCM in order to titrate the compounds in MeCN and PhCN solution. For solutions in DCM or $PhNO_2$, $SbCl_5$ solutions in the respective solvent were used. In all cases the oxidant solution was added using a microliter pipette (Eppendorf).

For compound **1** the monocation spectra were calculated using the comproportionation constant *K* in the following procedure:

$$K = e^{\frac{|\Delta E|F}{RT}}$$

$$\varepsilon = \frac{\varepsilon' (2 + \sqrt{K})}{\sqrt{K}}$$

$$f = \frac{\varepsilon}{\varepsilon''}$$

with ε' = extinction coefficient of a spectrum with maximum IV-CT band at an arbitrary wavenumber $\tilde{\nu}$ (usually one at the lower energy side of the IV-CT band)

ε'' = extinction coefficient at the wavenumber $\tilde{\nu}$ of a spectrum where the dication does not contribute significantly. This spectrum is obtained at a very early stage of titration when only little oxidant has been added.

$\Delta E_{1/2}$ = difference of half wave potentials of the first and second oxidation (see Tab. S1, for the measurement in $PhNO_2$ the $\Delta E_{1/2}$ value in DCM was used)

ε = corrected extinction coefficient of the monocation at wavenumber $\tilde{\nu}$

The monocation spectra result from the multiplication of the spectrum from which ε'' was determined with the factor *f*.

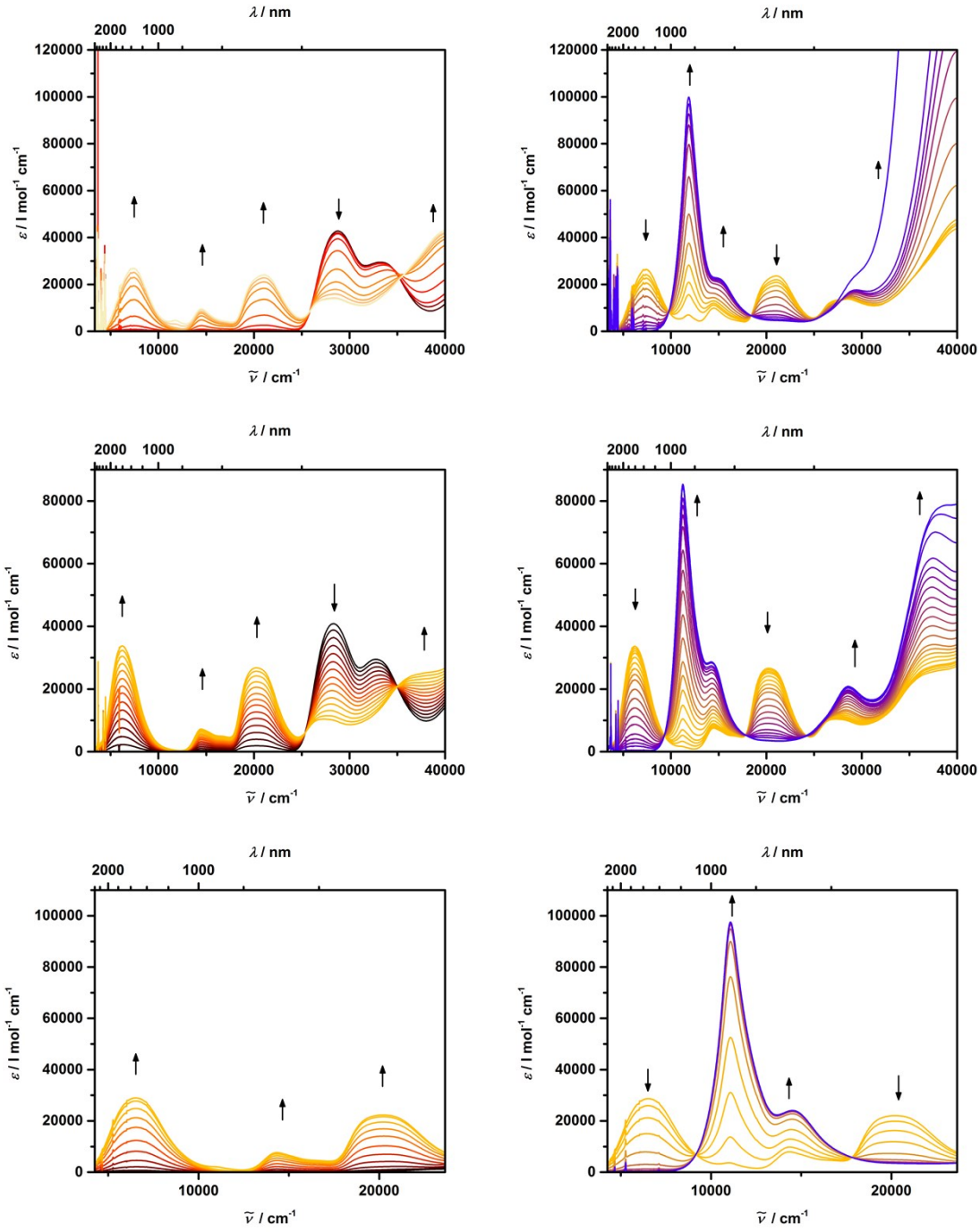

Figure S2: Redox titration of compound **1**. Top row: compound **1** in MeCN titrated with $SbCl_5$ in DCM. Middle row: compound **1** in DCM titrated with $SbCl_5$ in DCM. Bottom row: compound **1** in $PhNO_2$ titrated with $SbCl_5$ in $PhNO_2$.

For compound **2** and **3** the monocation spectra were calculated assuming that the monocation band posseses half the height of the dication band (both at ~14000 cm^{-1}).

$$\varepsilon_{max}^{+} = \frac{\varepsilon_{max}^{2+}}{2}$$

$$f = \frac{\varepsilon_{max}^{+}}{\varepsilon^{+}}$$

with ε_{max}^{+} = extinction coefficient of the maximum monocation band

ε_{max}^{2+} = extinction coefficient of the maximum dication band

ε^{+} = extinction coefficient of the monocation band in one of the first recorded spectra which shows almost no dication contribution

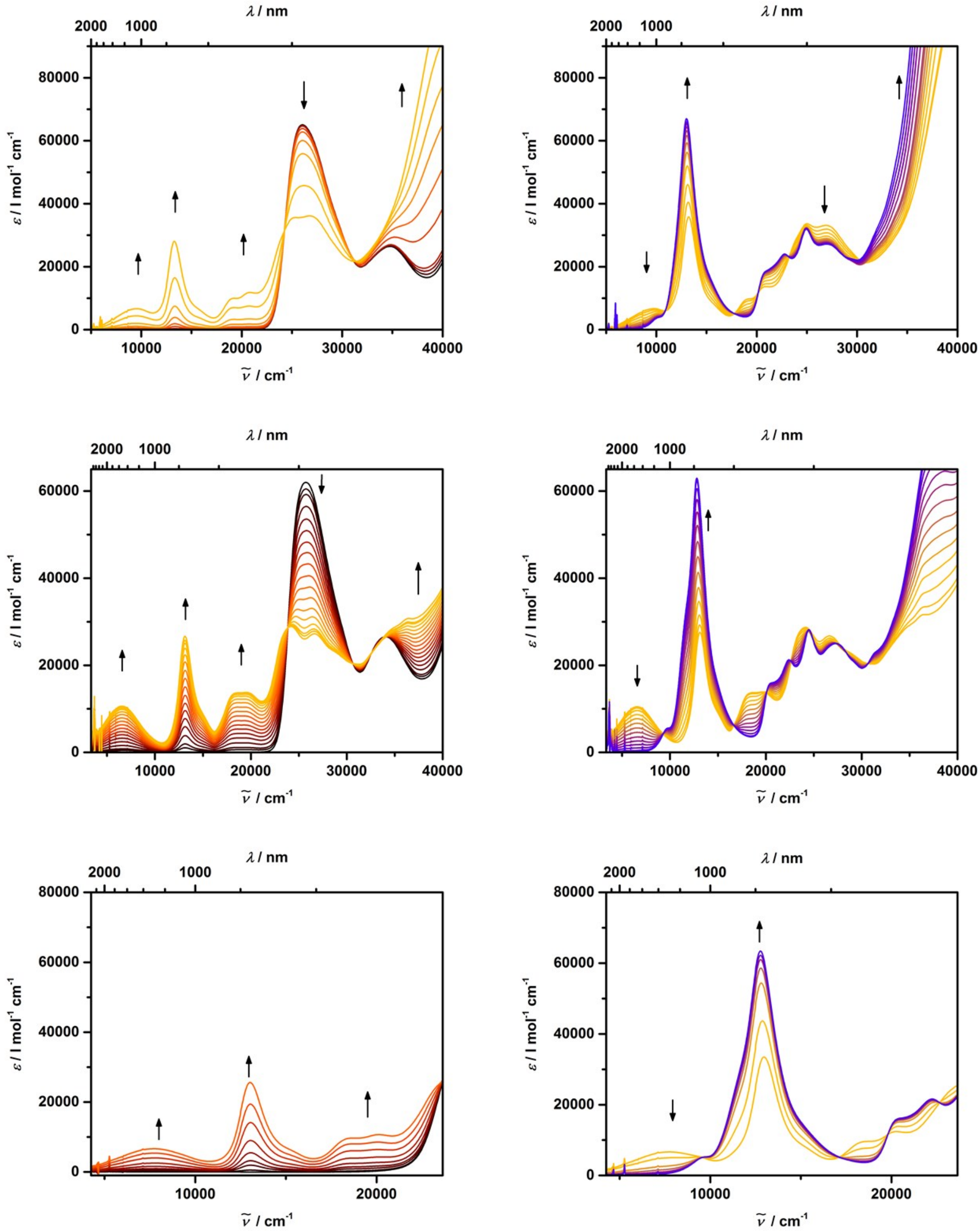
λ / nm
2000
1000
ε / l mol⁻¹ cm⁻¹
ṽ / cm⁻¹
0
20000
40000
60000
80000
10000
30000

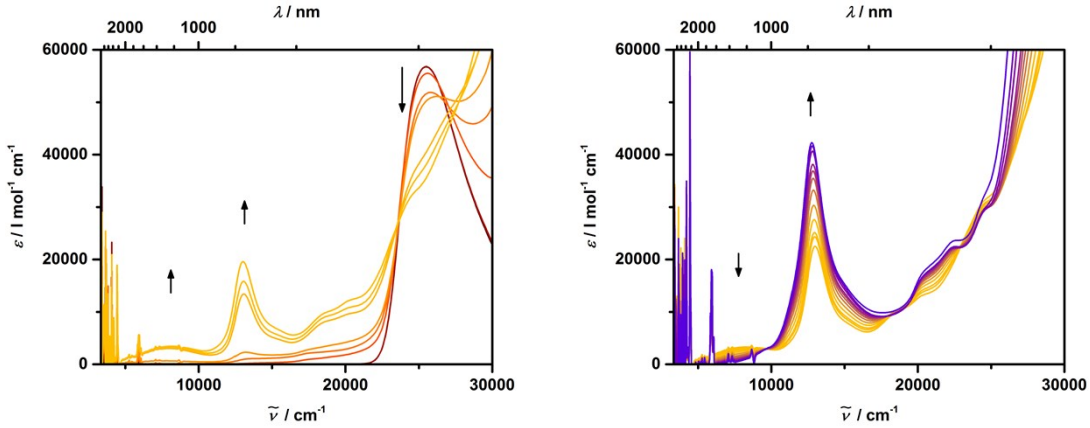

Figure S3: Redox titration of compound **2**. First row: compound **2** in MeCN titrated with $SbCl_5$ in DCM. Second row: compound **2** in DCM titrated with $SbCl_5$ in DCM. Third row: compound **2** in $PhNO_2$ titrated with $SbCl_5$ in $PhNO_2$. Fourth row: compound **2** in PhCN titrated with $SbCl_5$ in DCM.

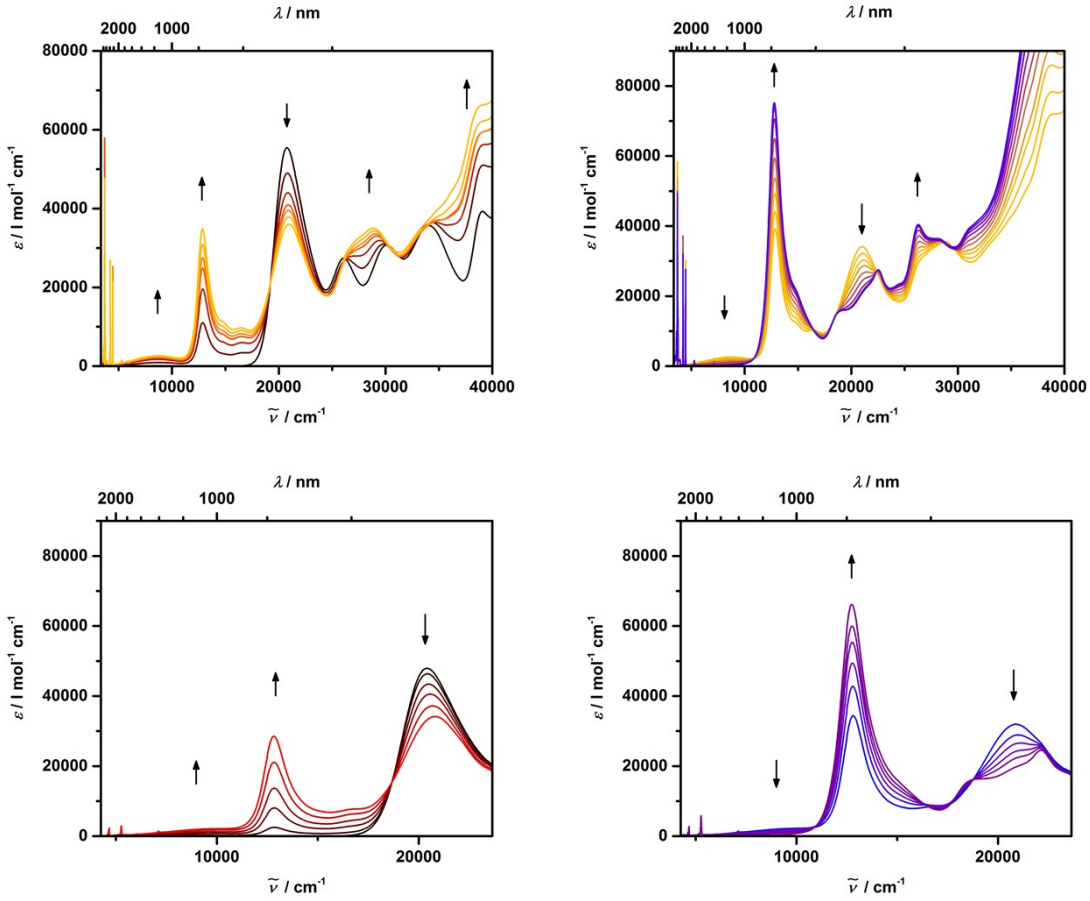

Figure S4: Redox titration of compound **3**. Upper row: compound **3** in DCM titrated with $SbCl_5$ in DCM. Bottom row: compound **3** in $PhNO_2$ titrated with $SbCl_5$ in $PhNO_2$.

Femtosecond Transient Absorption Spectroscopy

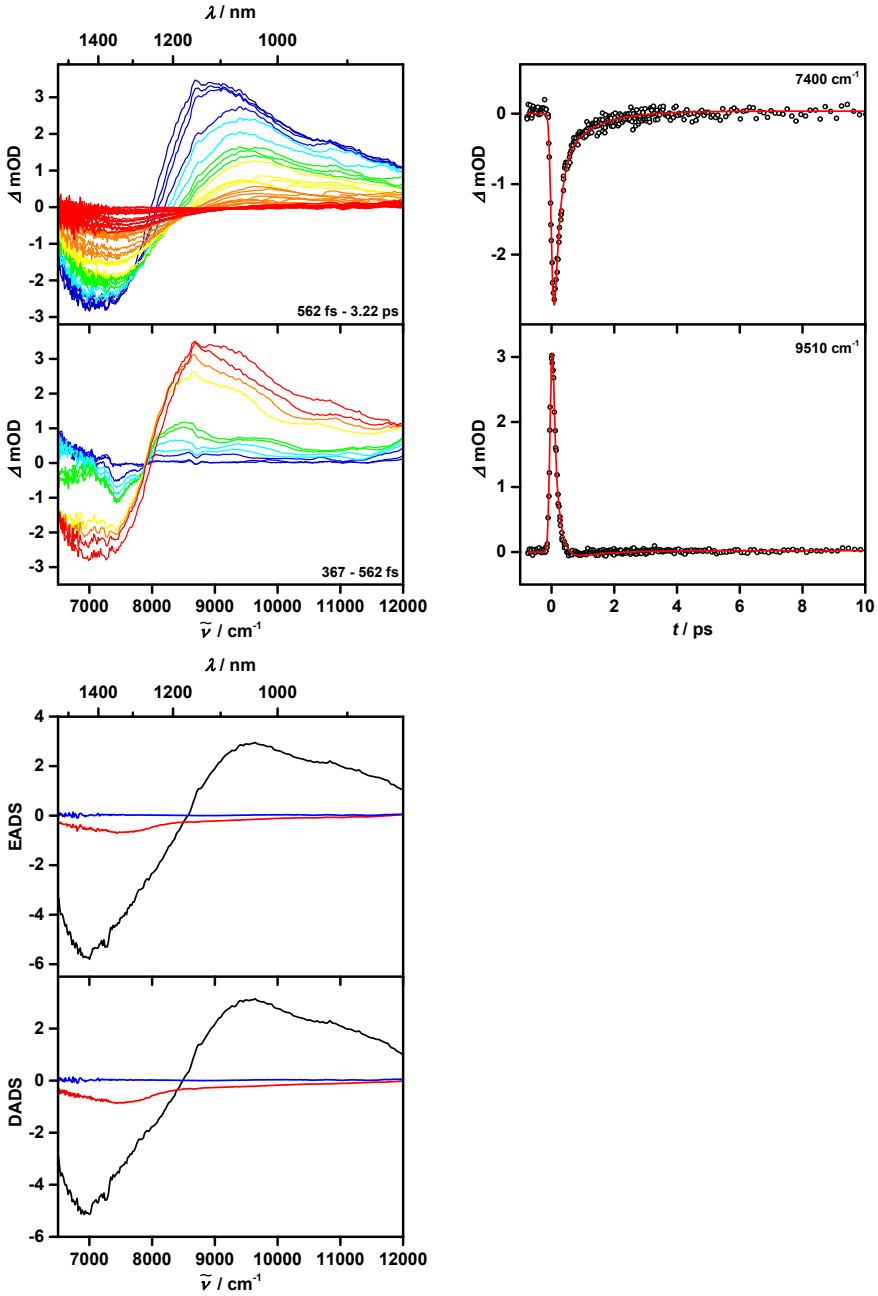

Figure S5: Upper panel left hand side: chirp-corrected transient absorption spectra of **1**$^{+}$ in DCM at 6270 cm^{-1} excitation wavenumber for different time regimes (temporal evolution blue to red spectra). Upper panel right hand side: time scans at selected wavenumbers together with the global fit traces. Lower panel: decay associated difference spectra (DADS) and evolution associated difference spectra (EADS) as results of a global fit.

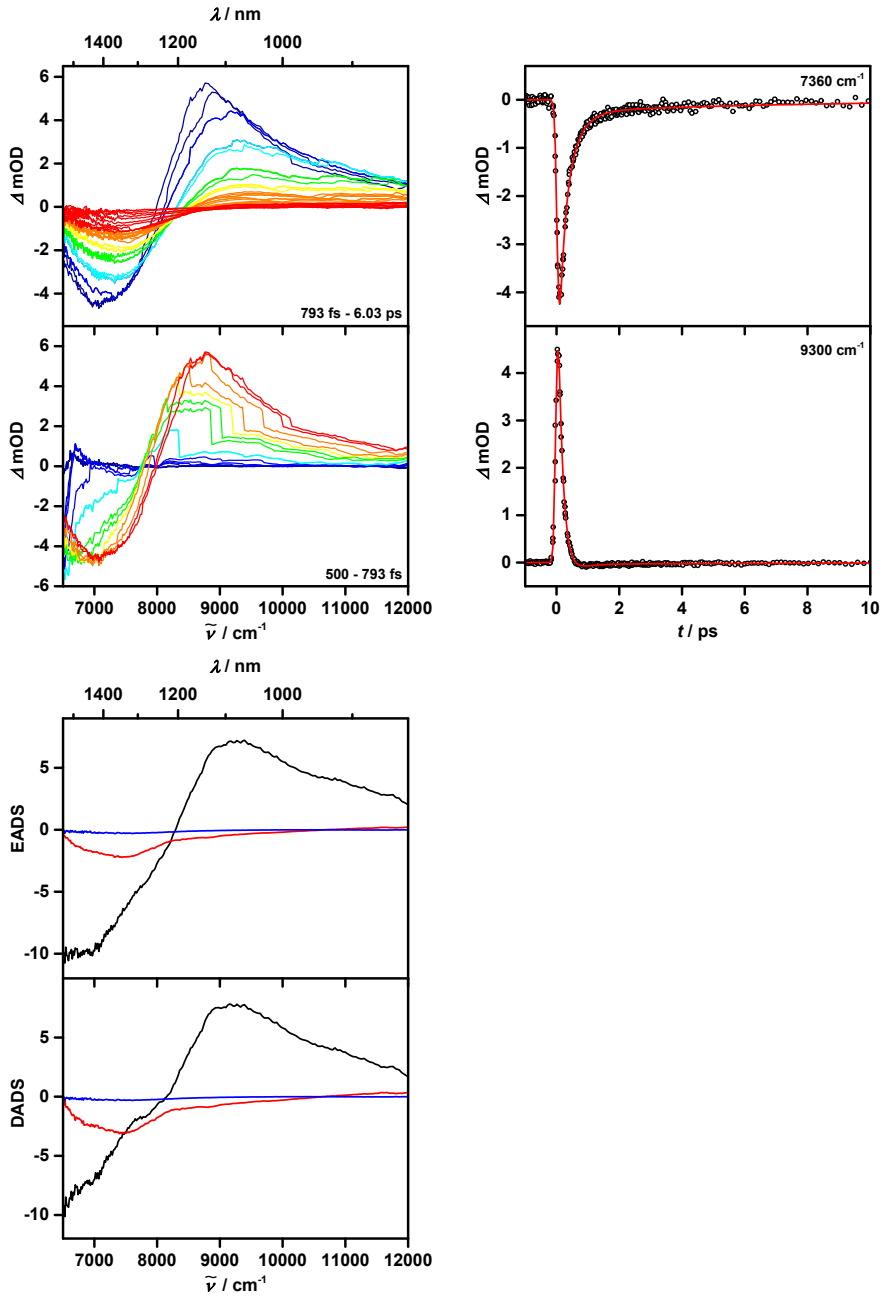

Figure S6: Upper panel left hand side: chirp-corrected transient absorption spectra of **1**$^{+}$ in $PhNO_2$ at 6510 cm^{-1} excitation wavenumber for different time regimes (temporal evolution blue to red spectra). Upper panel right hand side: time scans at selected wavenumbers together with the global fit traces. Lower panel: decay associated difference spectra (DADS) and evolution associated difference spectra (EADS) as results of a global fit.

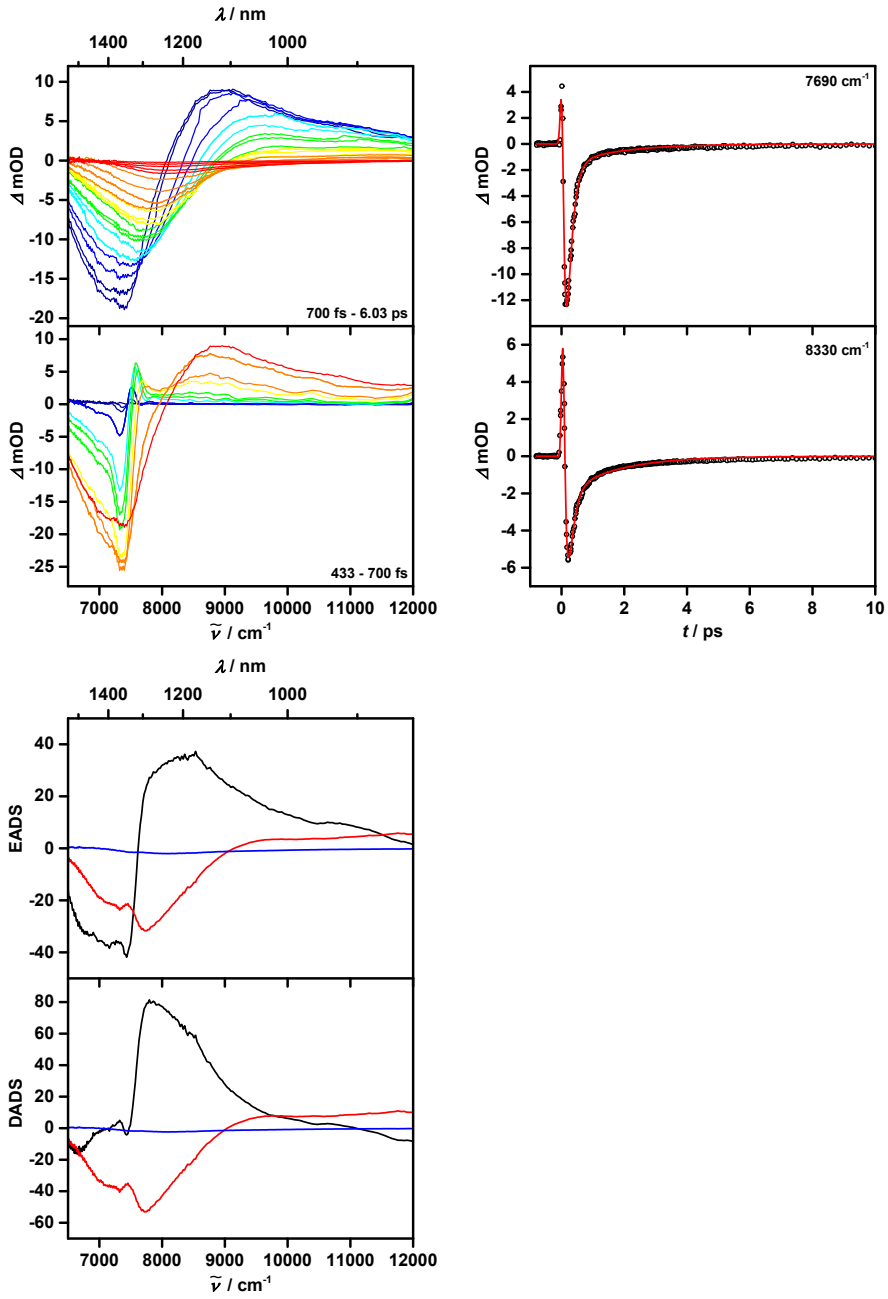

Figure S7: Upper panel left hand side: chirp-corrected transient absorption spectra of **1**$^{+}$ in MeCN at 7410 cm^{-1} excitation wavenumber for different time regimes (temporal evolution blue to red spectra). Upper panel right hand side: time scans at selected wavenumbers together with the global fit traces. Lower panel: decay associated difference spectra (DADS) and evolution associated difference spectra (EADS) as results of a global fit.

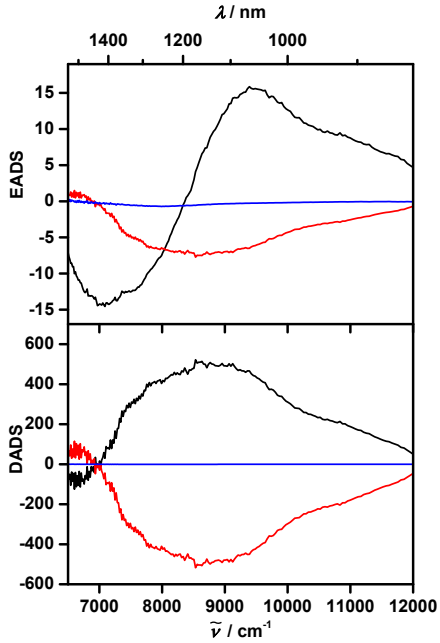

Figure S8: Decay associated difference spectra (DADS) and evolution associated difference spectra (EADS) as results of a global fit of **1**$^{+}$ in MeCN upon excitation at 6250 cm^{-1}.

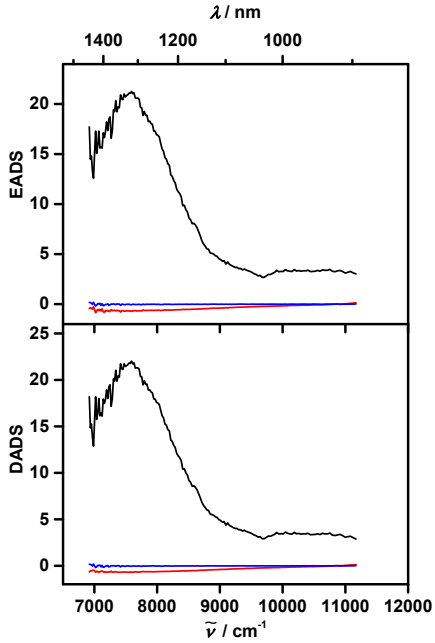

Figure S9: Decay associated difference spectra (DADS) and evolution associated difference spectra (EADS) as results of a global fit of $\mathbf{2}^{+}$ in DCM upon excitation at 6690 cm^{-1}.

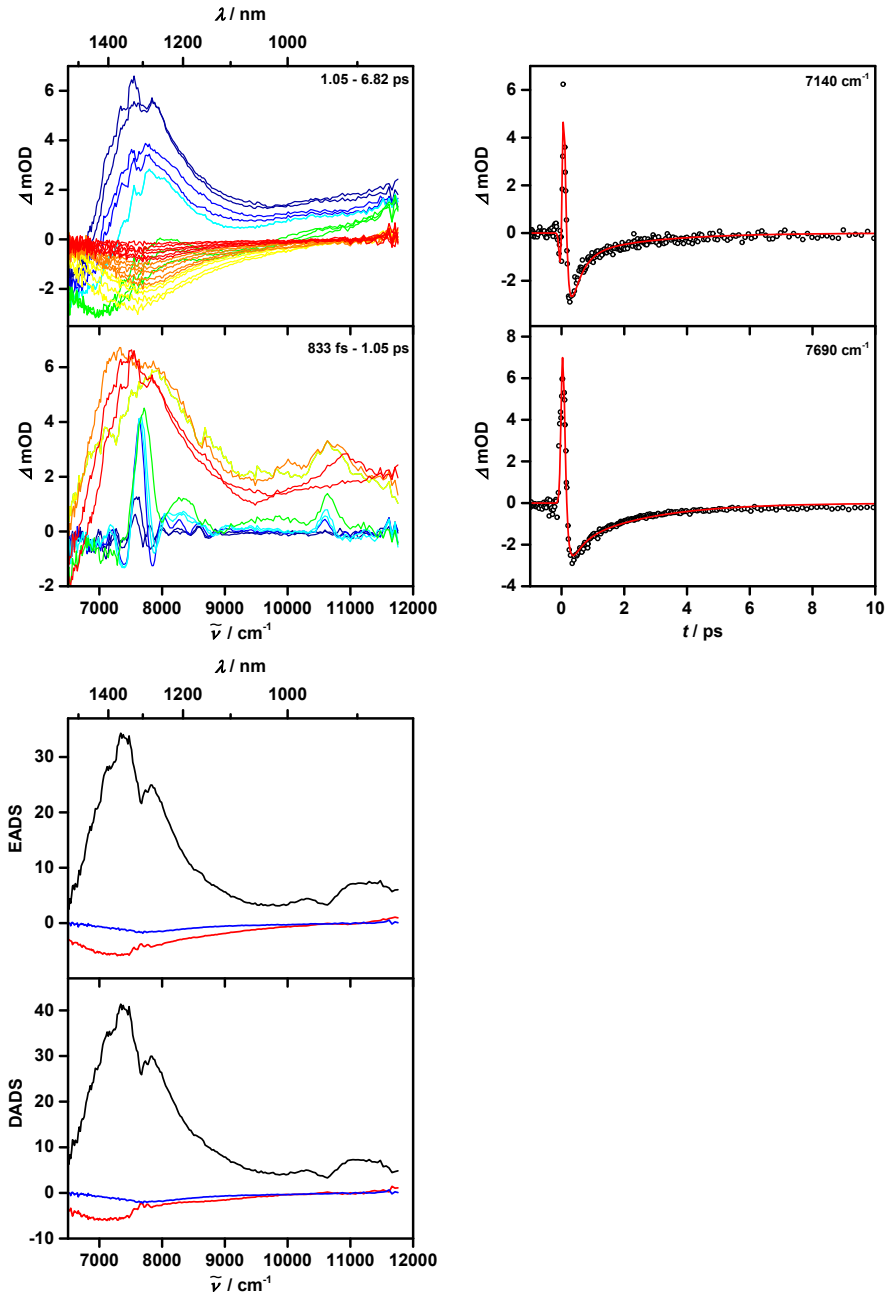

Figure S10: Upper panel left hand side: chirp-corrected transient absorption spectra of **2**$^{+}$ in DCM at 7500 cm^{-1} excitation wavenumber for different time regimes (temporal evolution blue to red spectra). Upper panel right hand side: time scans at selected wavenumbers together with the global fit traces. Lower panel: decay associated difference spectra (DADS) and evolution associated difference spectra (EADS) as results of a global fit.

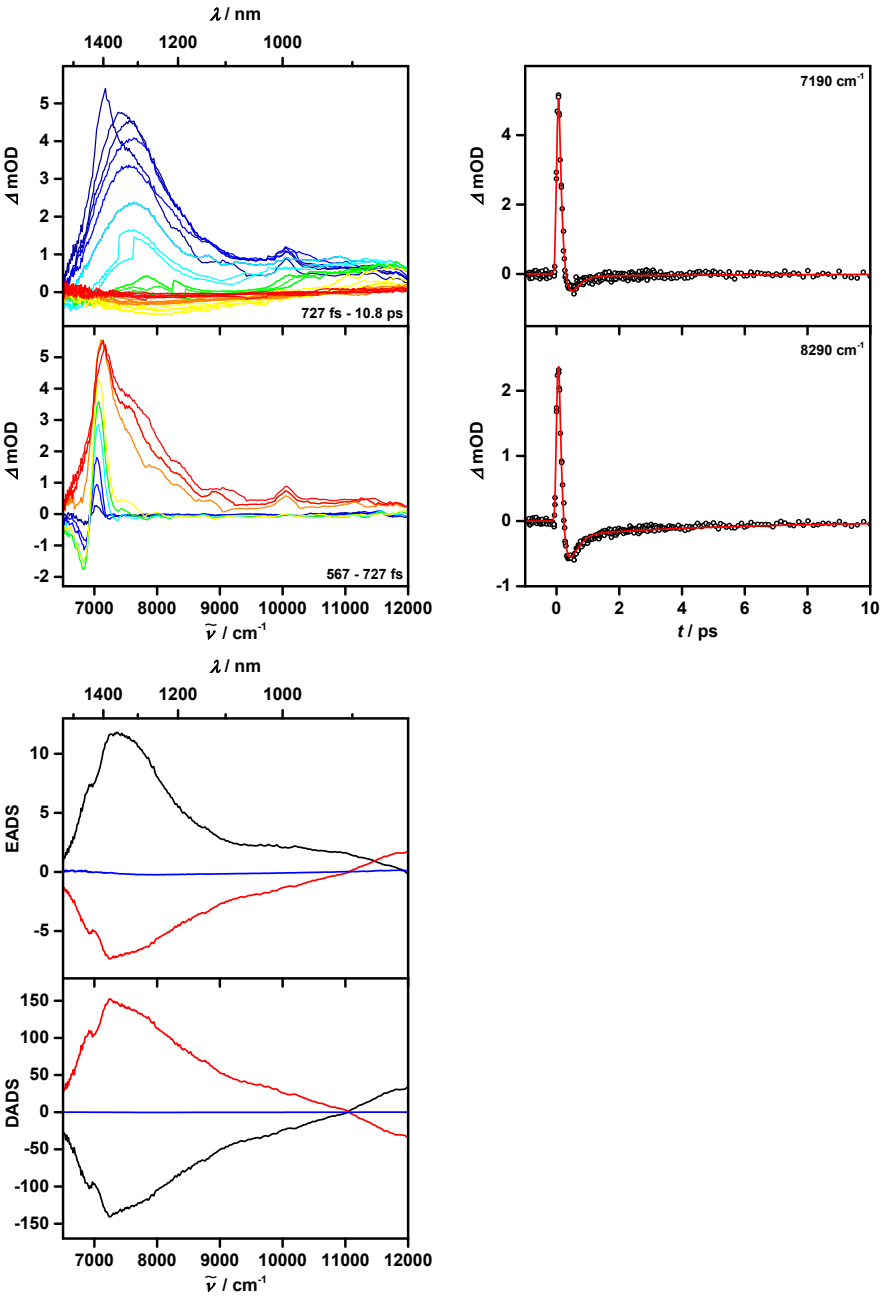

Figure S11: Upper panel left hand side: chirp-corrected transient absorption spectra of **2**$^{+}$ in $PhNO_2$ at 6690 cm^{-1} excitation wavenumber for different time regimes (temporal evolution blue to red spectra). Upper panel right hand side: time scans at selected wavenumbers together with the global fit traces. Lower panel: decay associated difference spectra (DADS) and evolution associated difference spectra (EADS) as results of a global fit.

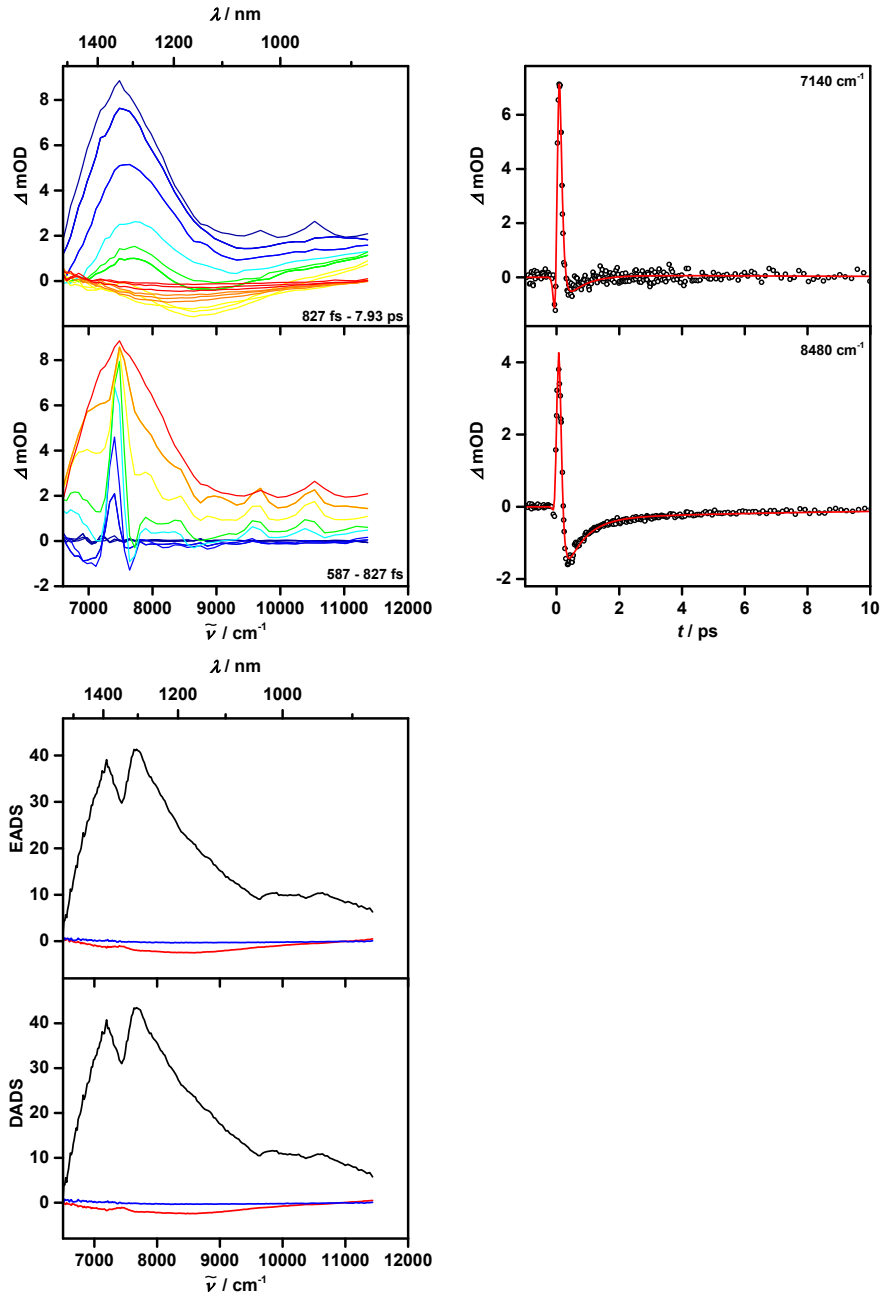

Figure S12: Upper panel left hand side: chirp-corrected transient absorption spectra of **2**$^{+}$ in PhCN at 7400 cm^{-1} excitation wavenumber for different time regimes (temporal evolution blue to red spectra). Upper panel right hand side: time scans at selected wavenumbers together with the global fit traces. Lower panel: decay associated difference spectra (DADS) and evolution associated difference spectra (EADS) as results of a global fit.

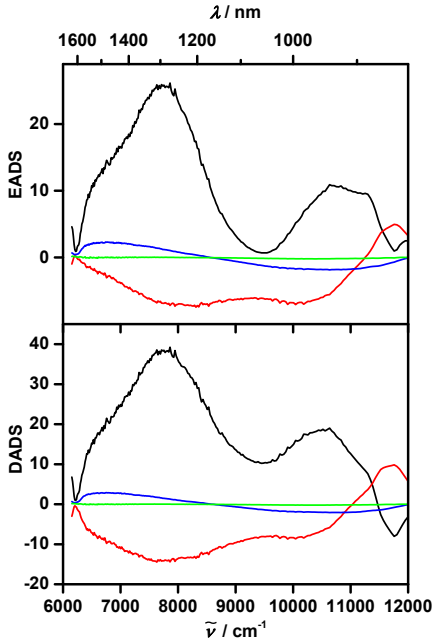

Figure S13: Decay associated difference spectra (DADS) and evolution associated difference spectra (EADS) as results of a global fit of **2**$^{+}$ in MeCN upon excitation at 8330 cm^{-1}.

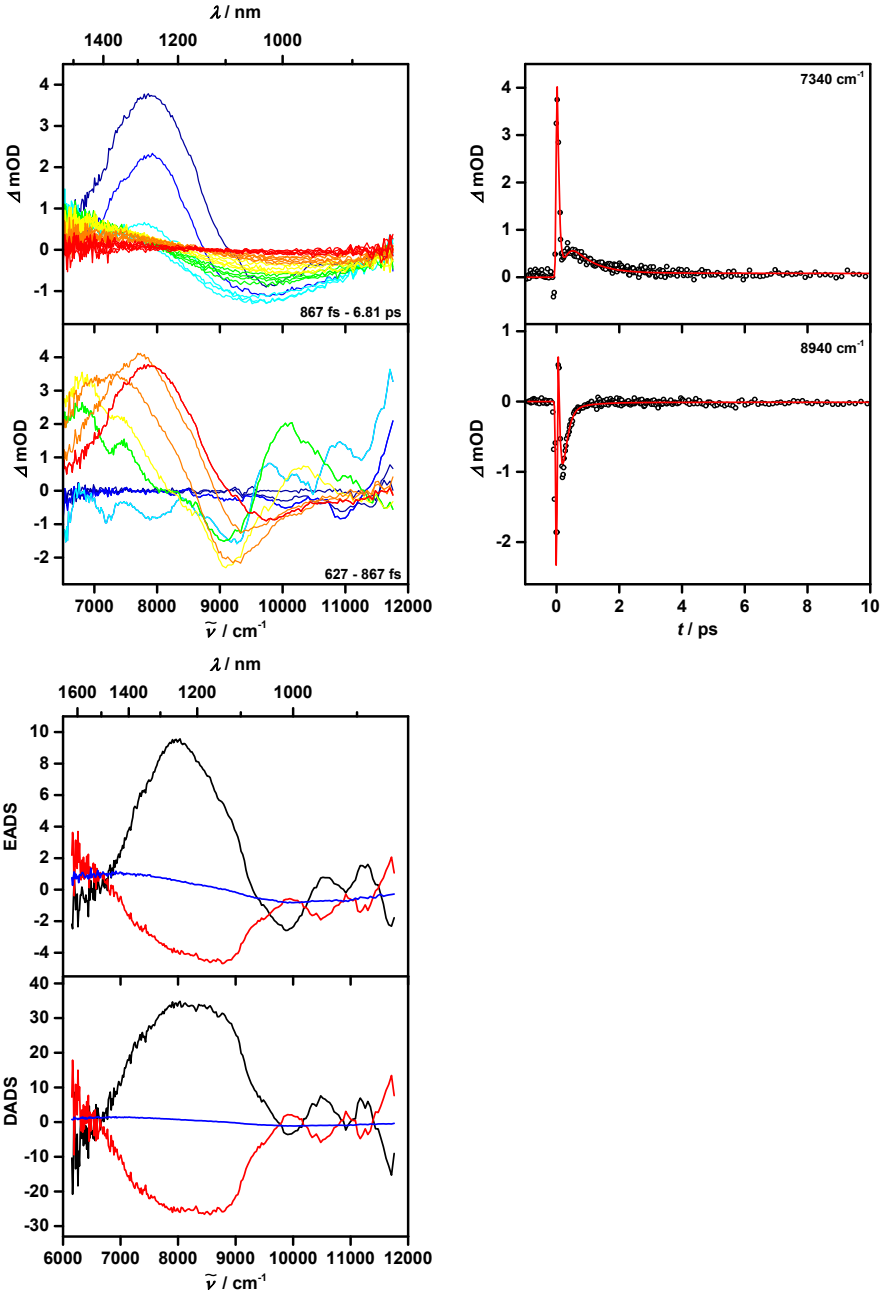

Figure S14: Upper panel left hand side: chirp-corrected transient absorption spectra of **2**$^{+}$ in MeCN at 9400 cm^{-1} excitation wavenumber for different time regimes (temporal evolution blue to red spectra). Upper panel right hand side: time scans at selected wavenumbers together with the global fit traces. Lower panel: decay associated difference spectra (DADS) and evolution associated difference spectra (EADS) as results of a global fit.

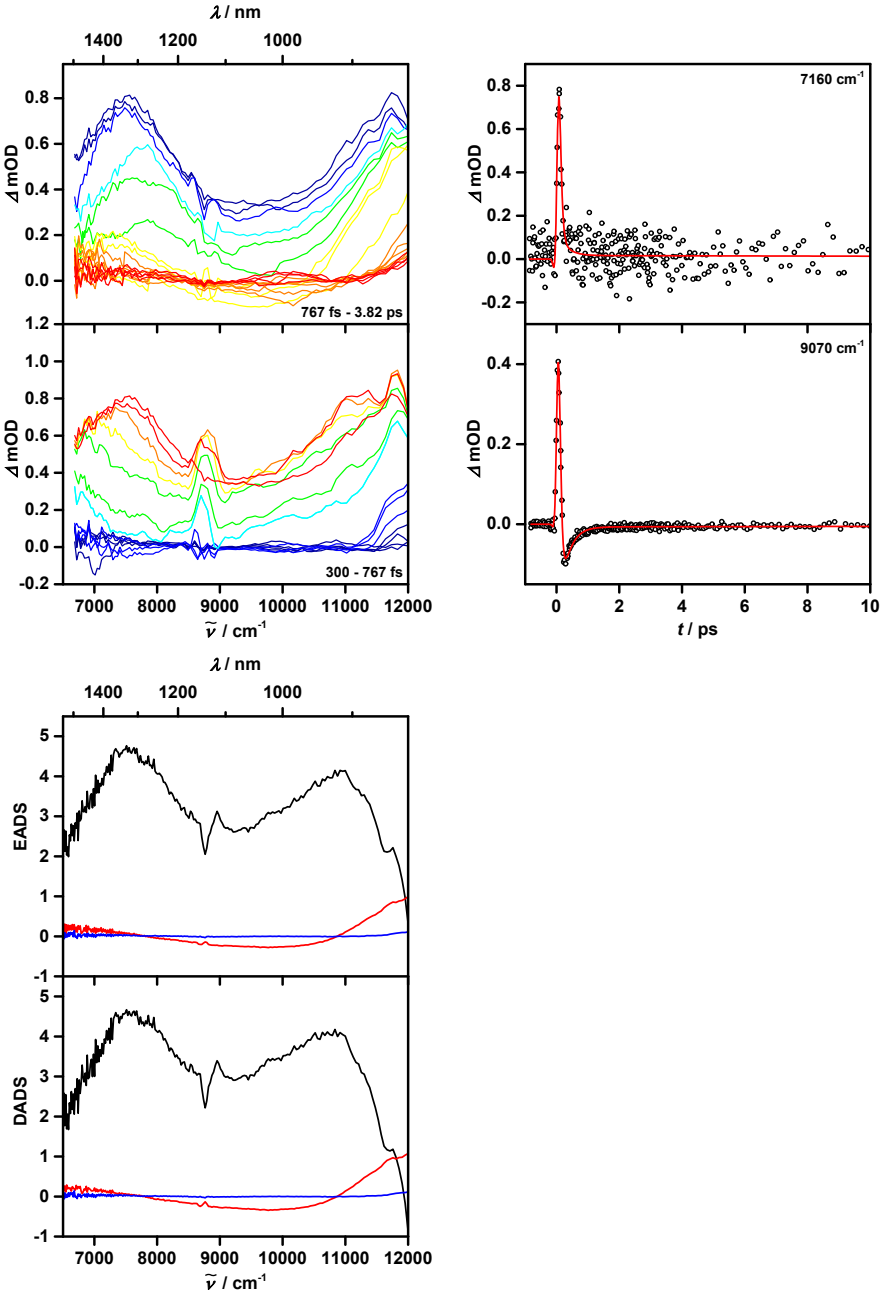

Figure S15: Upper panel left hand side: chirp-corrected transient absorption spectra of **3**$^{+}$ in DCM at 8770 cm^{-1} excitation wavenumber for different time regimes (temporal evolution blue to red spectra). Upper panel right hand side: time scans at selected wavenumbers together with the global fit traces. Lower panel: decay associated difference spectra (DADS) and evolution associated difference spectra (EADS) as results of a global fit.

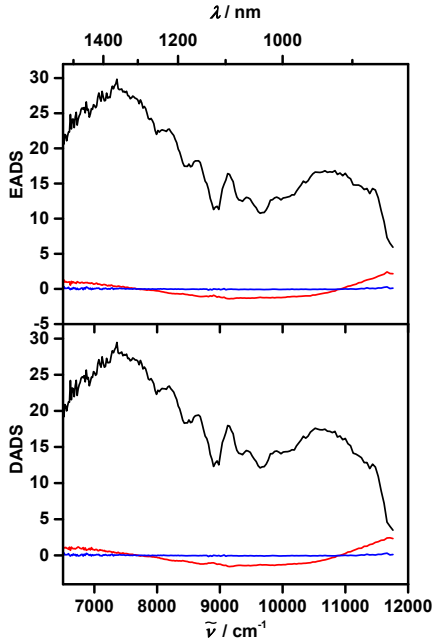

Figure S16: Decay associated difference spectra (DADS) and evolution associated difference spectra (EADS) as results of a global fit of **3**$^{+}$ in DCM at 8930 cm^{-1} excitation wavenumber

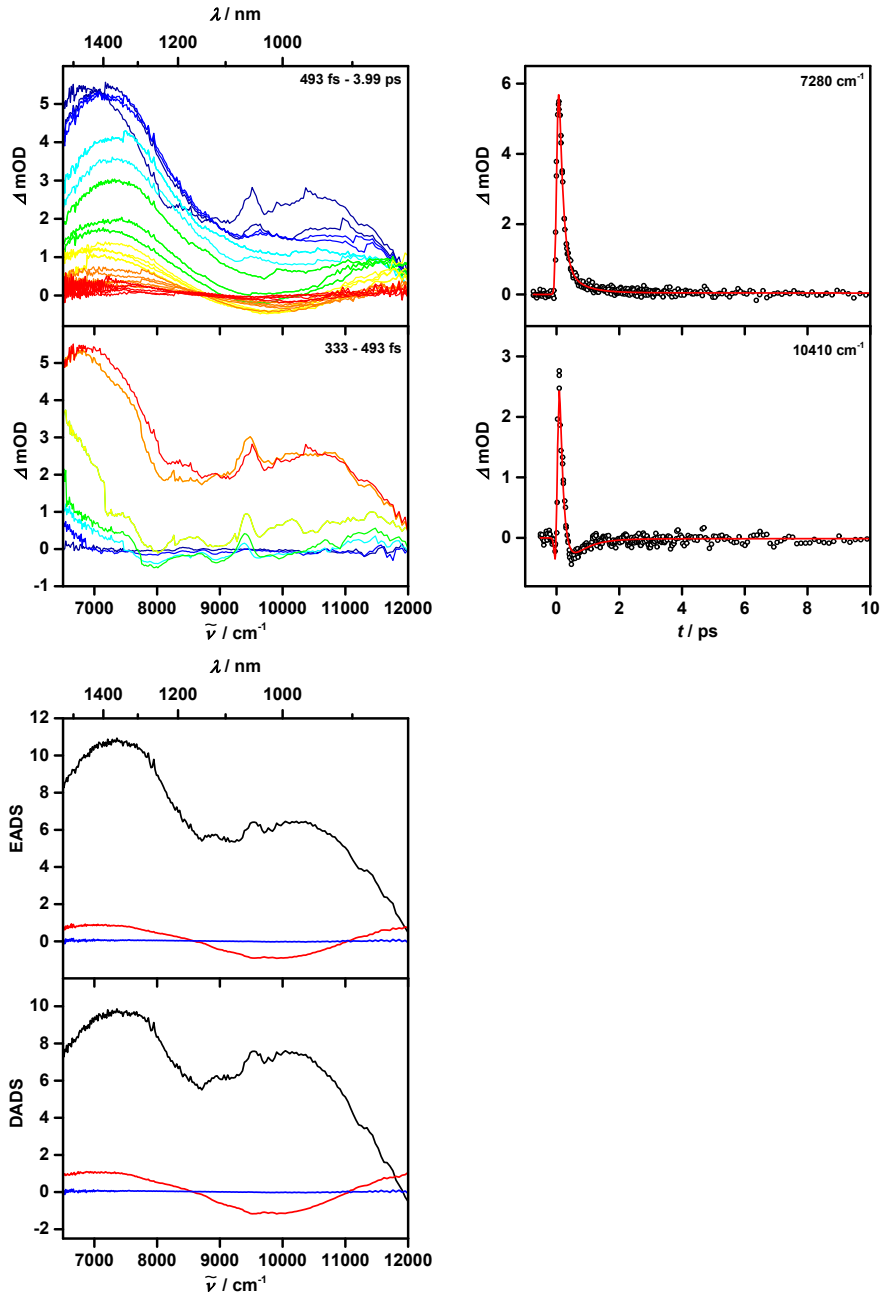

Figure S17: Upper panel left hand side: chirp-corrected transient absorption spectra of **3**$^{+}$ in $PhNO_2$ at 9430 cm^{-1} excitation wavenumber for different time regimes (temporal evolution blue to red spectra). Upper panel right hand side: time scans at selected wavenumbers together with the global fit traces. Lower panel: decay associated difference spectra (DADS) and evolution associated difference spectra (EADS) as results of a global fit.

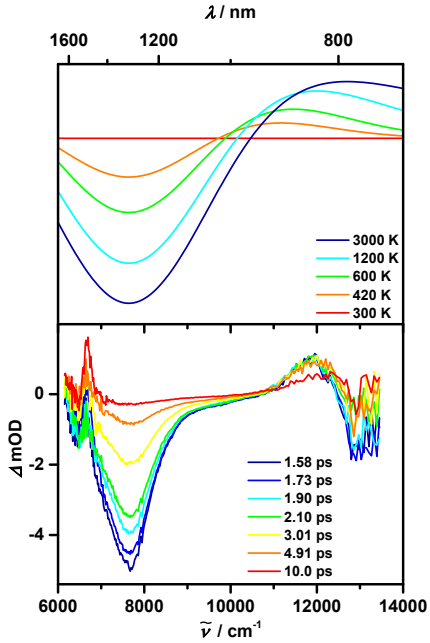

Figure S18: Computed difference spectra (upper panel) for different temperatures and experimental TA spectra (lower panel) at different delay times of **2**$^+$ in DCM@6690 cm^{-1}.

DFT computations

To evaluate the electronic coupling *V*, we applied the Mulliken-Hush approach[4,5] using the experimentally measured maximum energy of the IV-CT band, the transition moment from integration of the IV-CT band and the DFT computed dipole moment difference of the ground and the first excited state (see Table S2). The latter was computed at the density functional level, using a hybrid functional with 35% exact-exchange admixture, a SVP basis set and a polarizable continuum model accounting for solvent effects[6,7] using Gaussian09.[8] The time dependent (TD-DFT) calculations were done at the same level of theory.

Table S2. DFT computed and experimental IV-CT parameters for **1**$^+$-**3**$^+$ in DCM, $PhNO_2$ and MeCN.

		$\tilde{\nu}_{max}$ (exp)/ cm^{-1}	$\tilde{\nu}_{max}$ (theor)/ cm^{-1}	μ_{ab} (exp)/ D	μ_{ab} (theor)/ D	$\Delta\mu_{ab}$ / D	*V* (exp) / cm^{-1}	*V* (theor)/ cm^{-1}
DCM	**1**$^+$	6210	6139	12.9	18.2	1.31	3101	3068
	2$^+$	6586	6944	9.97	14.2	55.7	1110	1576
	3$^+$	8837	8026	4.35	8.12	77.8	491	820
$PhNO_2$	**1**$^+$	6574	5968	12.0	18.7	1.93	3276	2980
	2$^+$	7655	7902	8.80	12.2	56.8	1133	1559
	3$^+$	9863	9237	4.01	7.57	77.2	510	888
MeCN	**1**$^+$	7290	6444	12.0	17.6	1.71	3636	3218
	2$^+$	9402	8077	8.20	12.0	55.0	1344	1612
	3$^+$	--	--	--	--	--	--	--

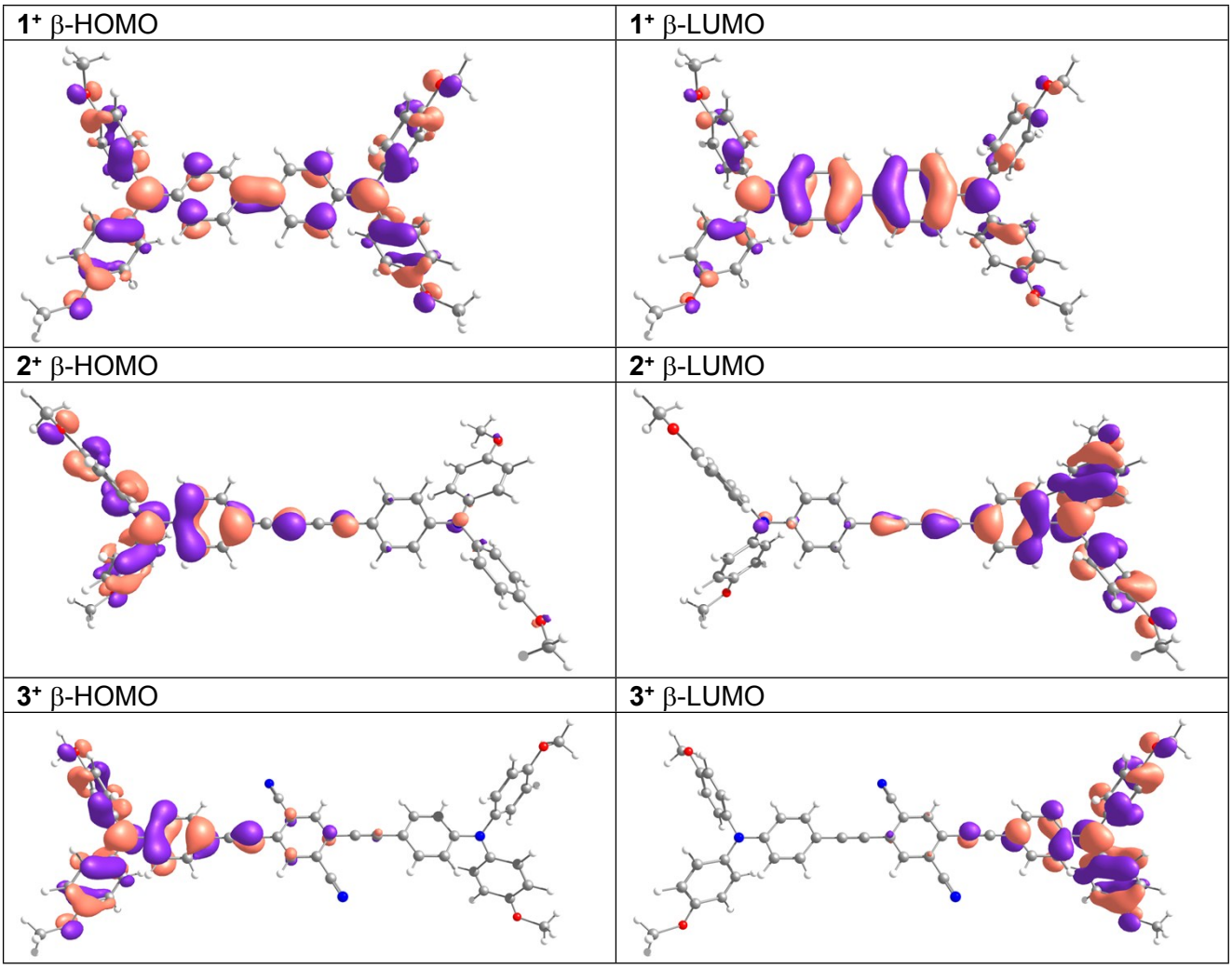

Figure S19: DFT computed orbitals in DCM which are relevant for the IV-CT excitation (β-HOMO→ β-LUMO).

References

1 C. Lambert and G. Nöll, *J. Am. Chem. Soc.*, 1999, **121**, 8434-8442.
2 J. Schäfer, B. Mladenova, D. R. Kattnig, M. Holzapfel, G. Grampp and C. Lambert, *Nature Chem.*, 2016, submitted.
3 S. Dümmling, E. Eichhorn, S. Schneider, B. Speiser and M. Würde, *Curr. Sep.*, 1996, **15**, 53-56.
4 C. Creutz, M. D. Newton and N. Sutin, *J. Photochem. Photobiol. A: Chem.*, 1994, **82**, 47-59.
5 N. Sutin, *Progr. Inorg. Chem.*, 1983, **30**, 441-498.
6 M. Renz, K. Theilacker, C. Lambert and M. Kaupp, *J. Am. Chem. Soc.*, 2009, **131**, 16292–16302.
7 M. Kaupp, M. Renz, M. Parthey, M. Stolte, F. Würthner and C. Lambert, *Phys. Chem. Chem. Phys.*, 2011, **13**, 16973-16986.
8 M. J. Frisch, G. W. Trucks, H. B. Schlegel, G. E. Scuseria, M. A. Robb, J. R. Cheeseman, G. Scalmani, V. Barone, B. Mennucci, G. A. Petersson, H. Nakatsuji, M. Caricato, X. Li, H. P. Hratchian, A. F. Izmaylov, J. Bloino, G. Zheng, J. L. Sonnenberg, M. Hada, M. Ehara, K. Toyota, R. Fukuda, J. Hasegawa, M. Ishida, T. Nakajima, Y. Honda, O. Kitao, H. Nakai,

T. Vreven, J. J. A. Montgomery, J. E. Peralta, F. Ogliaro, M. Bearpark, J. J. Heyd, E. Brothers, K. N. Kudin, V. N. Staroverov, T. Keith, R. Kobayashi, J. Normand, K. Raghavachari, A. Rendell, J. C. Burant, S. S. Iyengar, J. Tomasi, M. Cossi, N. Rega, J. M. Millam, M. Klene, J. E. Knox, J. B. Cross, V. Bakken, C. Adamo, J. Jaramillo, R. Gomperts, R. E. Stratmann, O. Yazyev, A. J. Austin, R. Cammi, C. Pomelli, J. W. Ochterski, R. L. Martin, K. Morokuma, V. G. Zakrzewski, G. A. Voth, P. Salvador, J. J. Dannenberg, S. Dapprich, A. D. Daniels, O. Farkas, J. B. Foresman, J. V. Ortiz, J. Cioslowski and D. J. Fox, Gaussian, Inc., Revision D.01 edn., 2010.